Supplementary Material

Dendritic Cell-Activating Magnetic Nanoparticles Enable Early Prediction of Anti-Tumor Response with Magnetic Resonance Imaging

Adam J. Grippin[†,2], Brandon Wummer[1], Tyler Wildes[1], Kyle Dyson[1], Vrunda Trivedi[1], Changlin Yang[1], Mathew Sebastian[1], Hector Mendez-Gomez[1], Suraj Padala[1], Mackenzie Grubb[2], Matthew Fillingim[1], Adam Monsalve[2], Elias J. Sayour[1,], Jon Dobson[2,3,*] and Duane A. Mitchell[1,*]*

[1] Preston A. Wells, Jr. Center for Brain Tumor Therapy, UF Brain Tumor Immunotherapy Program, Lillian S. Wells Department of Neurosurgery, McKnight Brain Institute, University of Florida, Gainesville, FL
[2] J. Crayton Pruitt Family Department of Biomedical Engineering, Herbert Wertheim College of Engineering, University of Florida, Gainesville, FL
[3] Department of Materials Science & Engineering, University of Florida, Gainesville, FL

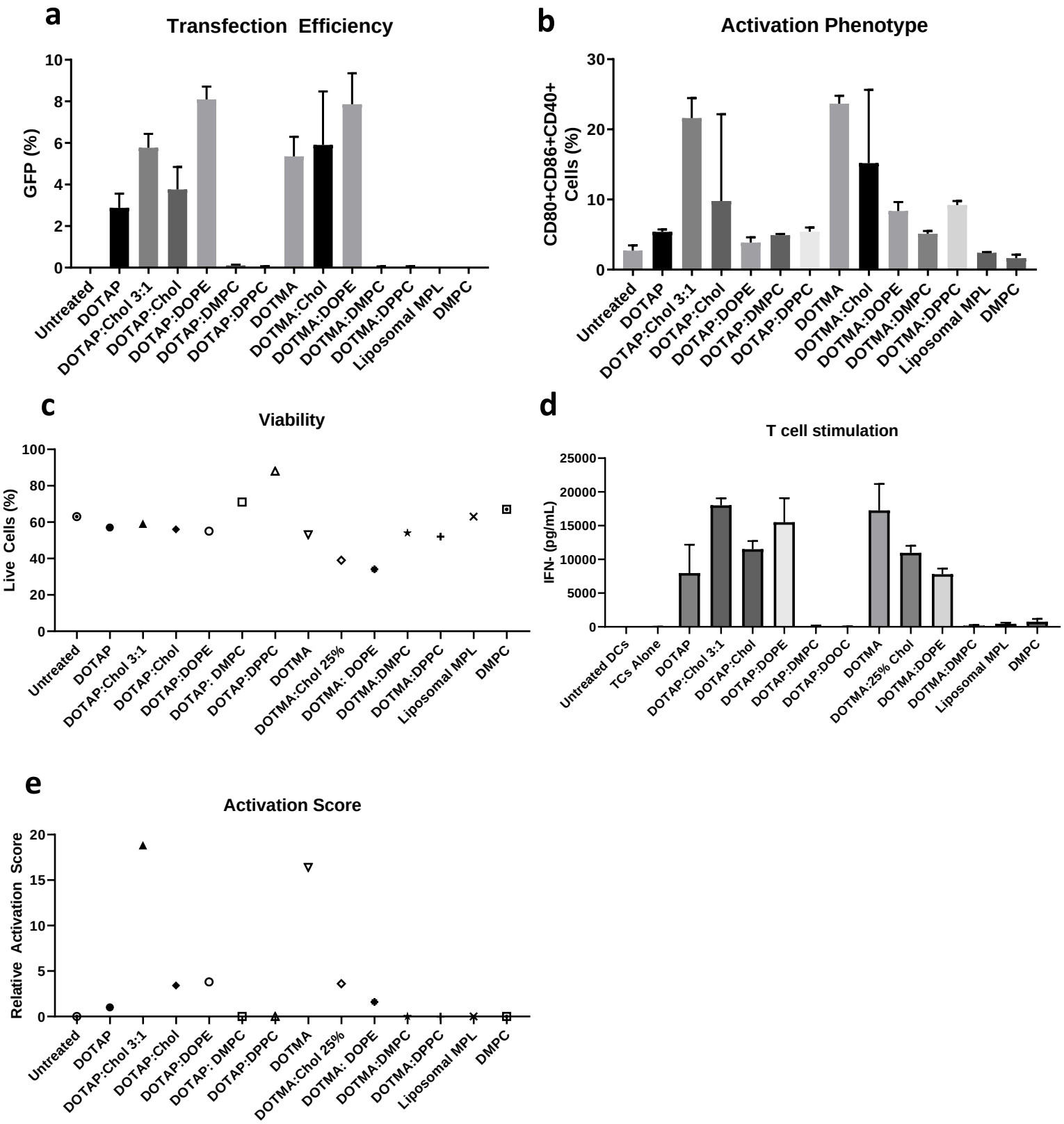

Supplementary Figure 1: Translatable nanoparticles transfect and activate DCs. a, GFP expression in BMDCs after 24 hour incubation with each RNA-loaded particle. **b,** Co-expression of CD40, CD80, and CD86 on BMDCs after 24 hour incubation with each particle construct. **c,** Viability of BMDCs after 24 hour incubation with each construct. **d,** BMDCs were loaded with IO-RNA-NPs bearing OVA RNA and incubated with OVA-specific OT1 T cells. T cell activation is displayed as IFN-γ assessed by ELISA. **e,** Relative Activation Score calculated as the product of average values for Viability, Transfection Efficiency, Activation, and T cell Stimulation for each formulation normalized to the score for DOTAP.

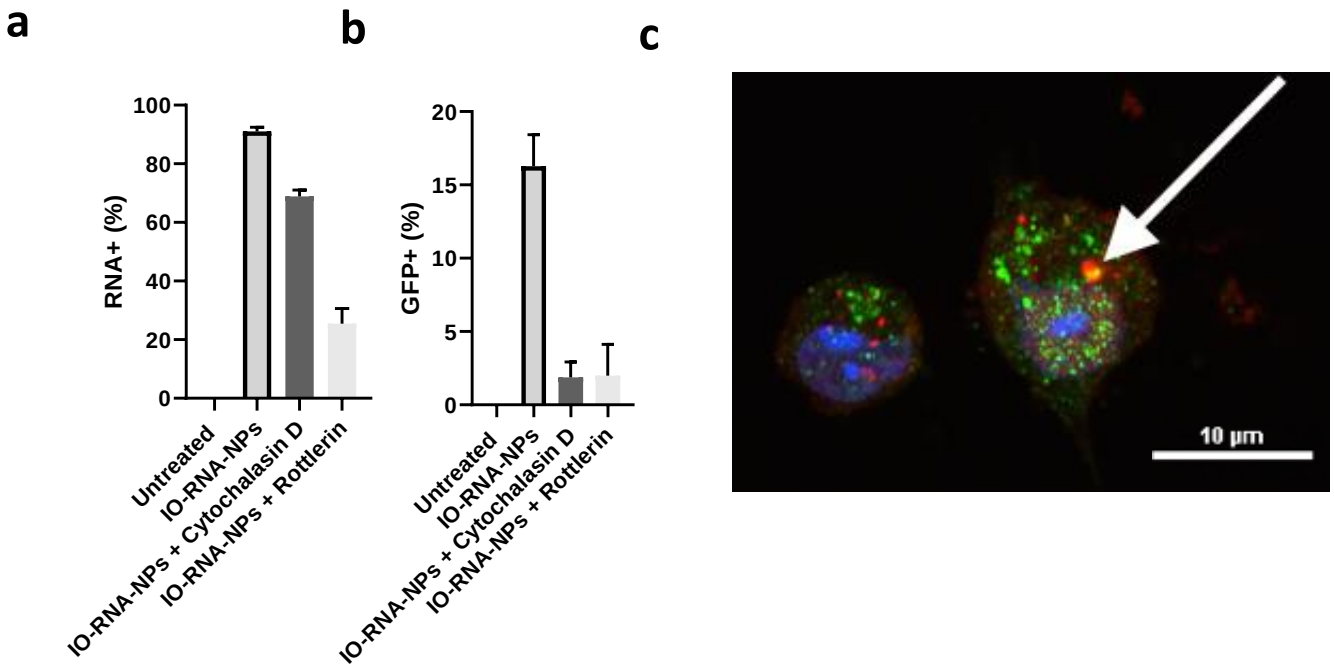

Supplementary Figure 2: IO-RNA-NPs are taken up by macropinocytosis. RNA uptake (a) and transfection efficiency (b) of DC2.4s treated with GFP-RNA-NP-NPs after pretreatment with rottlerin or cytochalasin D. **c,** Confocal microscopy demonstrating co-localization of Cy3-labelled IO-RNA-NPs (red) and TLR7 (green). Nuclei are marked with DAPI (blue).

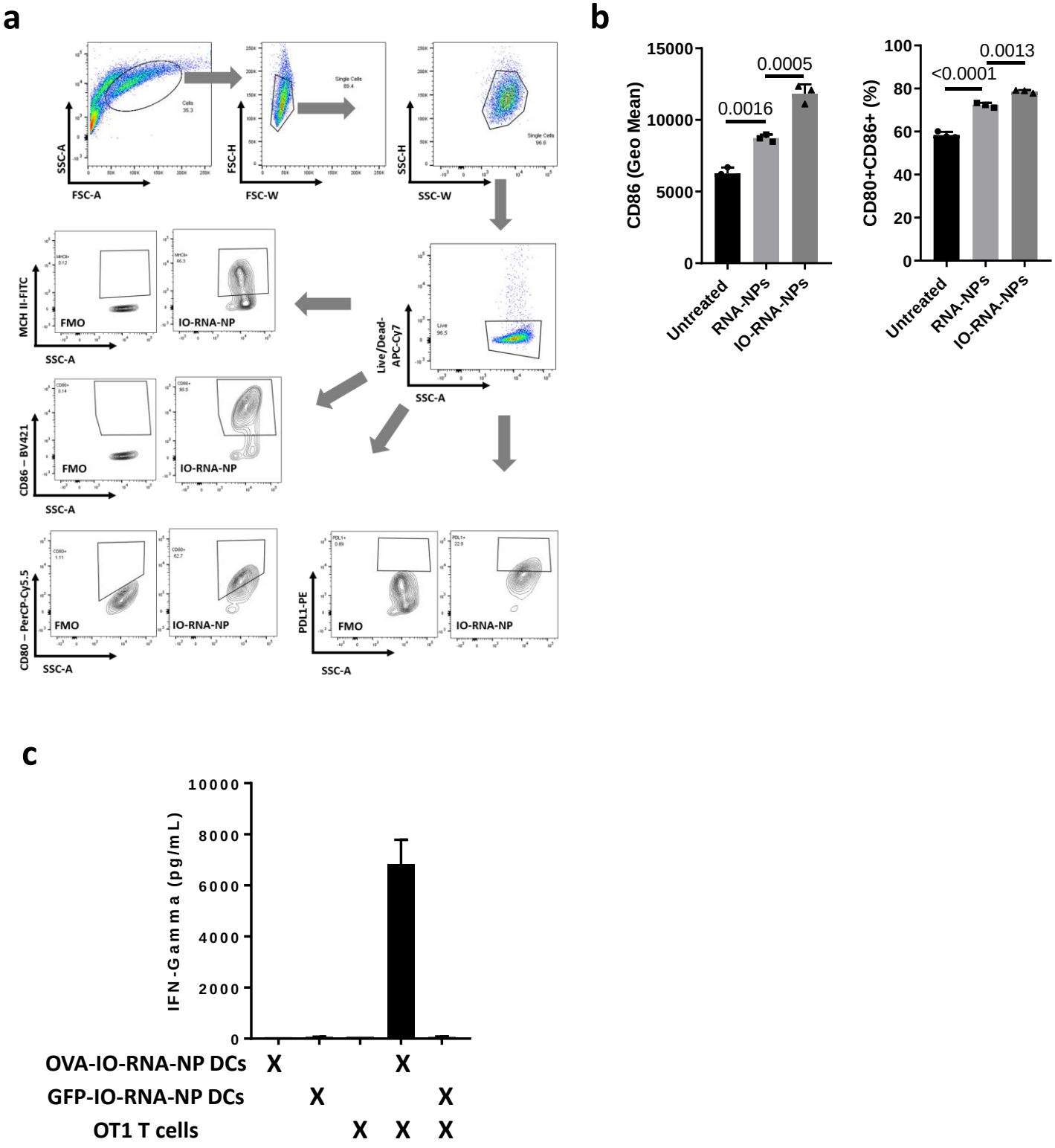

Supplementary Figure 3: IO-RNA-NPs induce antigen specific DC activation. a, Gating Strategy. Positive populations were selected using fluorescence minus one (FMO) controls. **b,** Expression of CD86 and co-expression of CD80 and CD86 on BMDCs after 24 hour incubation with RNA-NPs or IO-RNA-NPs. Data are plotted as geometric mean fluorescence intensity and percentages. One-way ANOVA and Tukey's tests were used for statistical comparisons. Numbers on graphs are *P* values. **c,** BMDCs were loaded with IO-RNA-NPs bearing either OVA RNA or GFP RNA and incubated with OVA-specific OT1 T cells. T cell activation is displayed as IFN-γ assessed by ELISA.

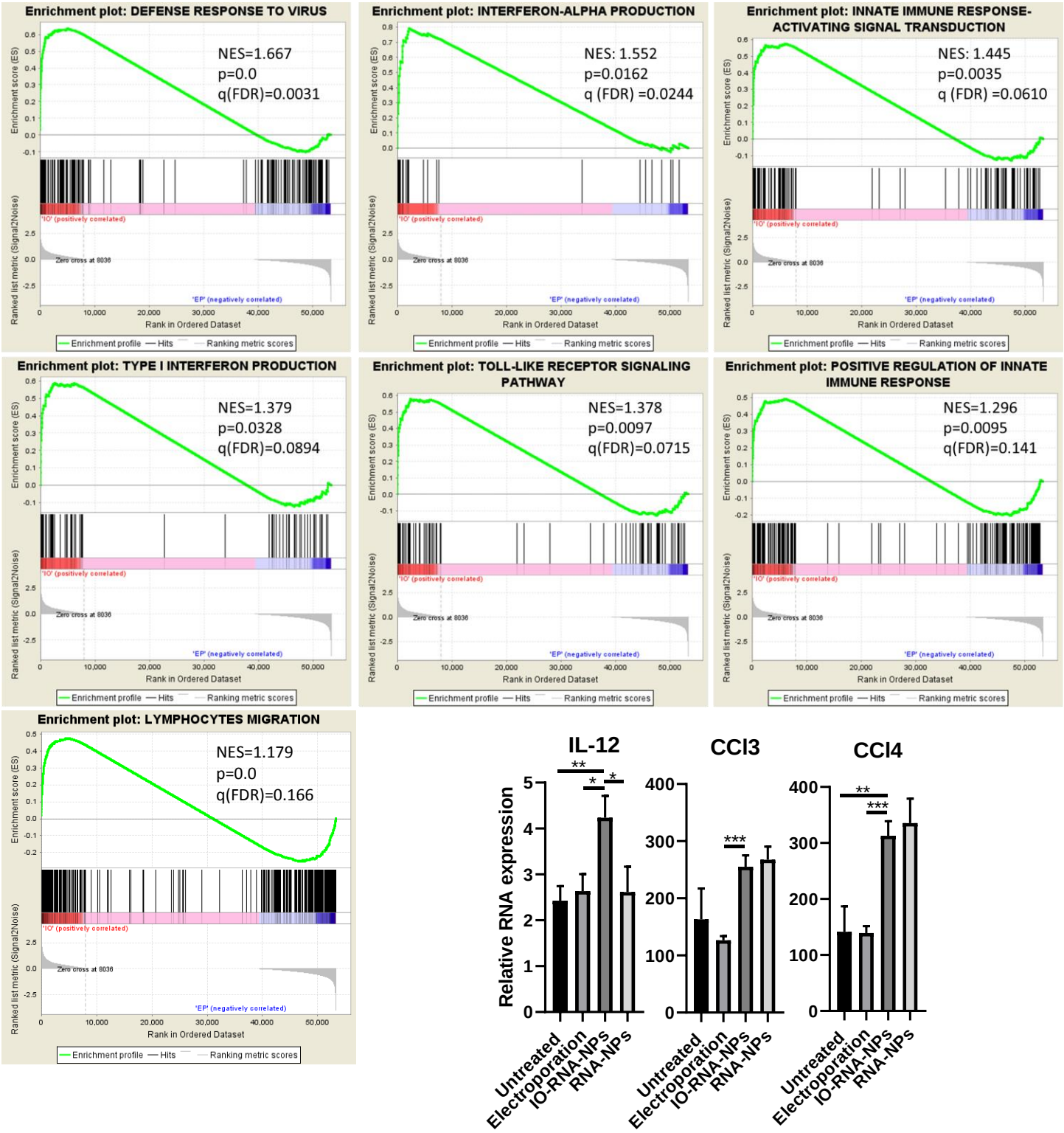

Supplementary Figure 4: IO-RNA-NPs induce expression of antiviral gene sets. Gene set enrichment plots for 7 gene sets relating to RNA uptake and processing in primary BMDCs 24 hours after treatment with GFP mRNA via either IO-RNA-NPs or electroporation. ***Bottom right:*** Individual comparisons of IL-12, CCL3, and CCL4 are included to demonstrate differences between all four treatment groups.

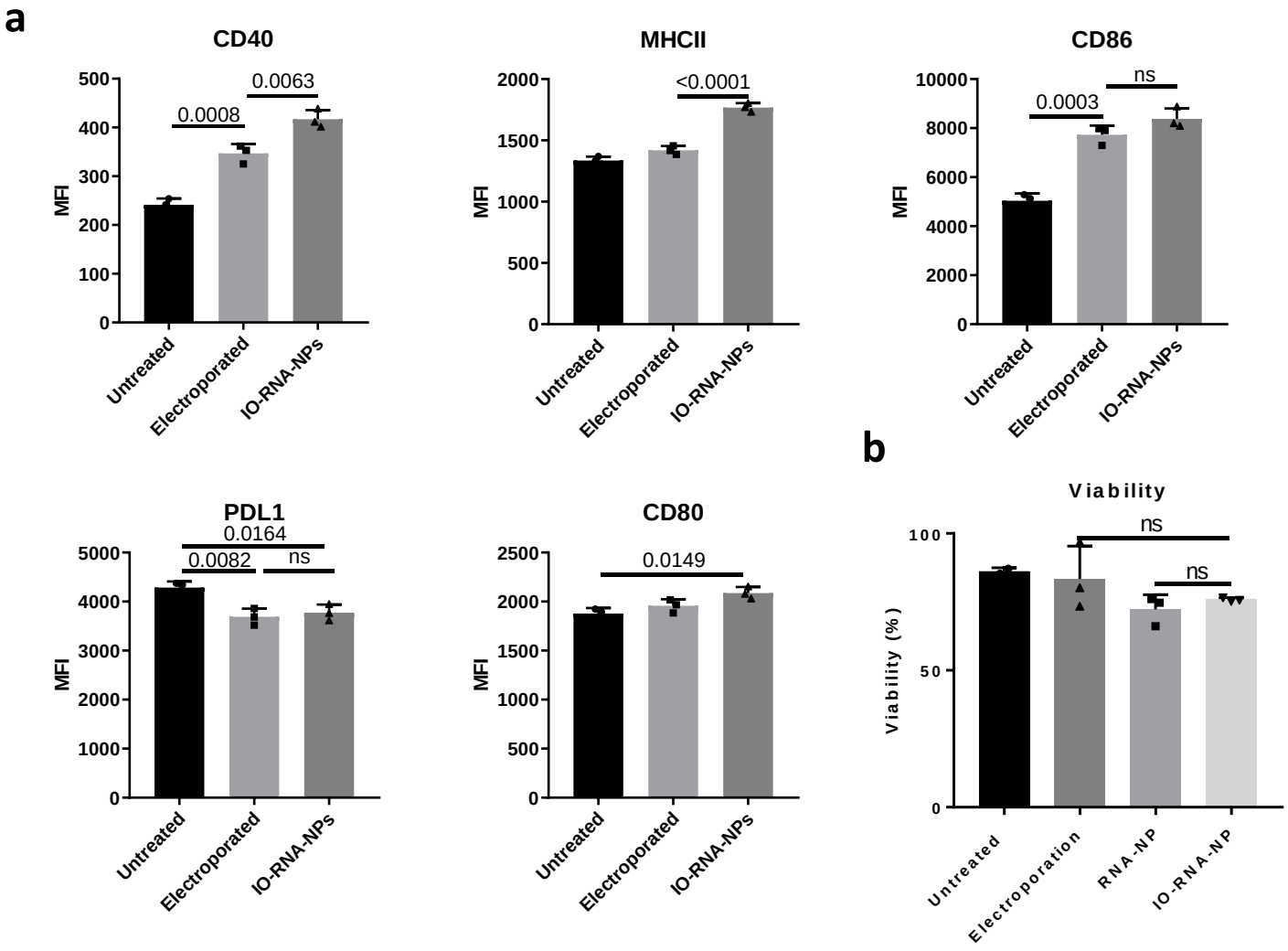

Supplementary Figure 5: IO-RNA-NPs enhance activation of BMDCs. a, Phenotypic markers of activation on BMDCs assessed by flow cytometry 24 hours after treatment with electroporation or IO-RNA-NPs. Data are presented as geometric mean fluorescence intensity. One-way ANOVA and Tukey's tests were used for statistical analysis (n=3). **b,** BMDC viability 24 hours after electroporation or incubation with RNA-NPs or IO-RNA-NPs as assessed by automated cell counter.

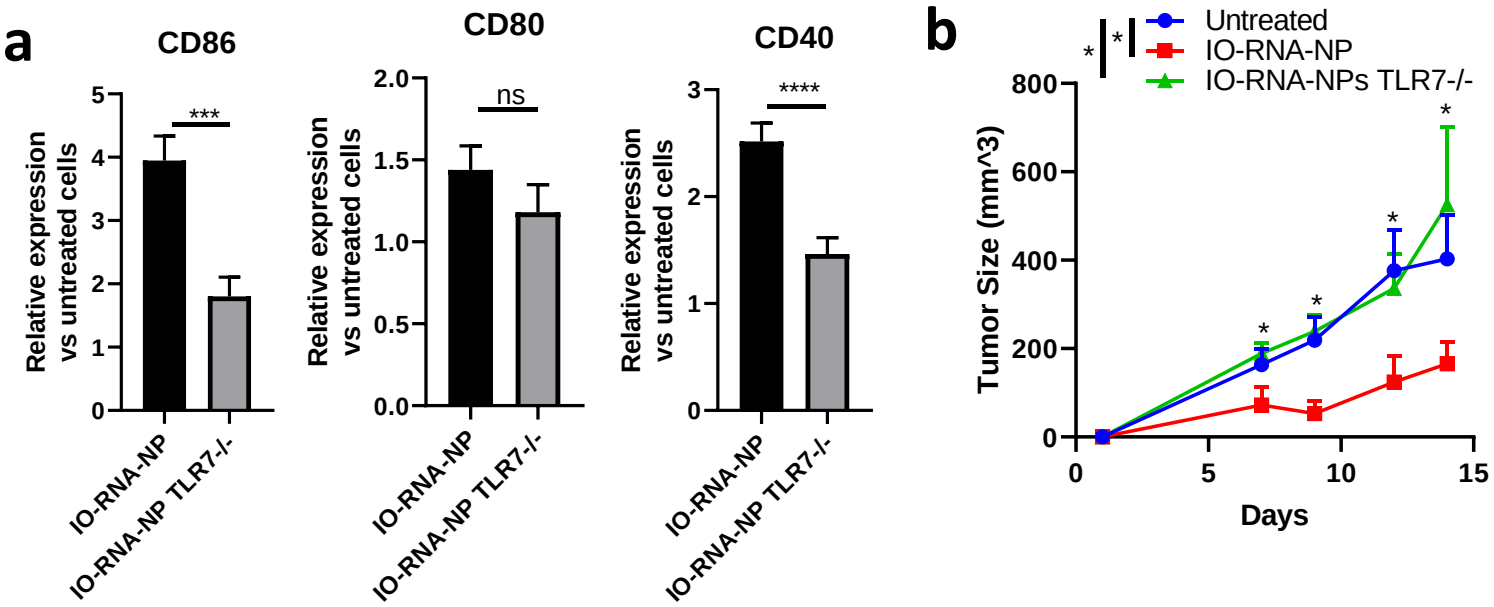

Supplementary Figure 6: Activating capacity of RNA-NPs is dependent on TLR7 activation. a, b, Expression of activation markers on DCs generated from C57Bl6 mice or TLR7-/- mice after treatment with IO-RNA-NPs. Expression of each marker is plotted as a ratio of geometric means between treated and untreated cells. Statistical analysis was completed with unpaired t tests. **b,** Tumor growth in C57Bl6 mice treated with OT1 T cells alone, with IO-RNA-NP DCs from C57Bl6 mice, or with IO-RNA-NP DCs from TLR7-/- mice. Comparisons over time are completed with ANOVA. Differences at individual timepoints were analyzed with Mann-Whitney tests for significance. *p<0.05, ***p<0.001, ****p<0.0001.

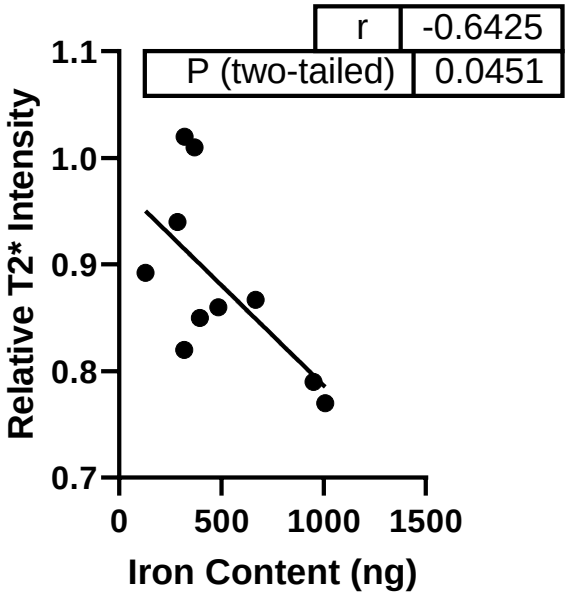

Supplementary Figure 7: T2*-weighted MRI intensity correlates with iron oxide content in LNs. Mice were imaged with MRI 24 hours after intradermal injections of IONPs (500ug, 250ug, 125ug, or 62.5ug). Iron oxide content in each vaccination site draining LN were then compared to relative intensities of those LNs.

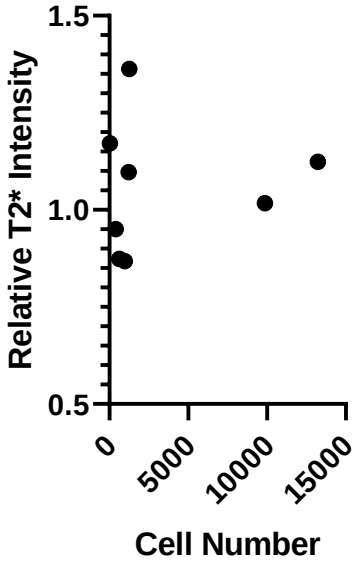

Supplementary Figure 8: T2*-weighted MRI intensity does not correlate with cell count in the absence of IONPs. Mice were imaged with MRI 48 hours after intradermal injections of RNA-electroporated DCs. Cell counts in each lymph node were obtained via flow cytometry immediately after MRI imaging.

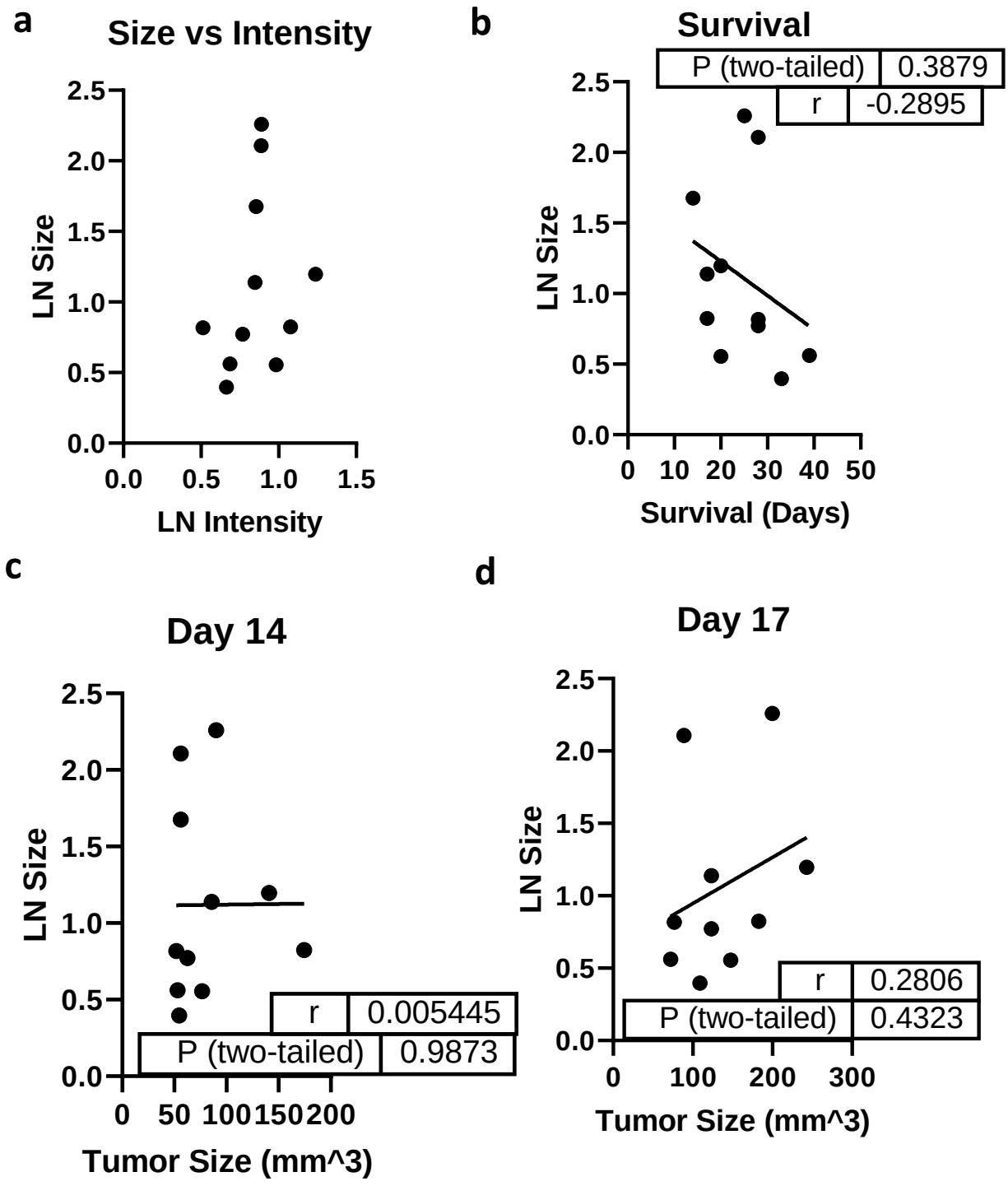

Supplementary Figure 9: LN size does not correlate strongly with efficacy. Mice were treated with DCs loaded with IO-RNA-NPs 5 days after subcutaneous injection of B16F10-OVA tumors. Mice were imaged with MRI 48 hours after treatment and tumor growth was followed over time. Relative lymph node (LN) size is plotted against relative LN intensity (**a**), survival (**b**), Day 14 tumor size (**c**) and Day 17 tumor size (**d**). Numbers on graphs are correlation coefficients and p values derived from Pearson's correlation coefficient.

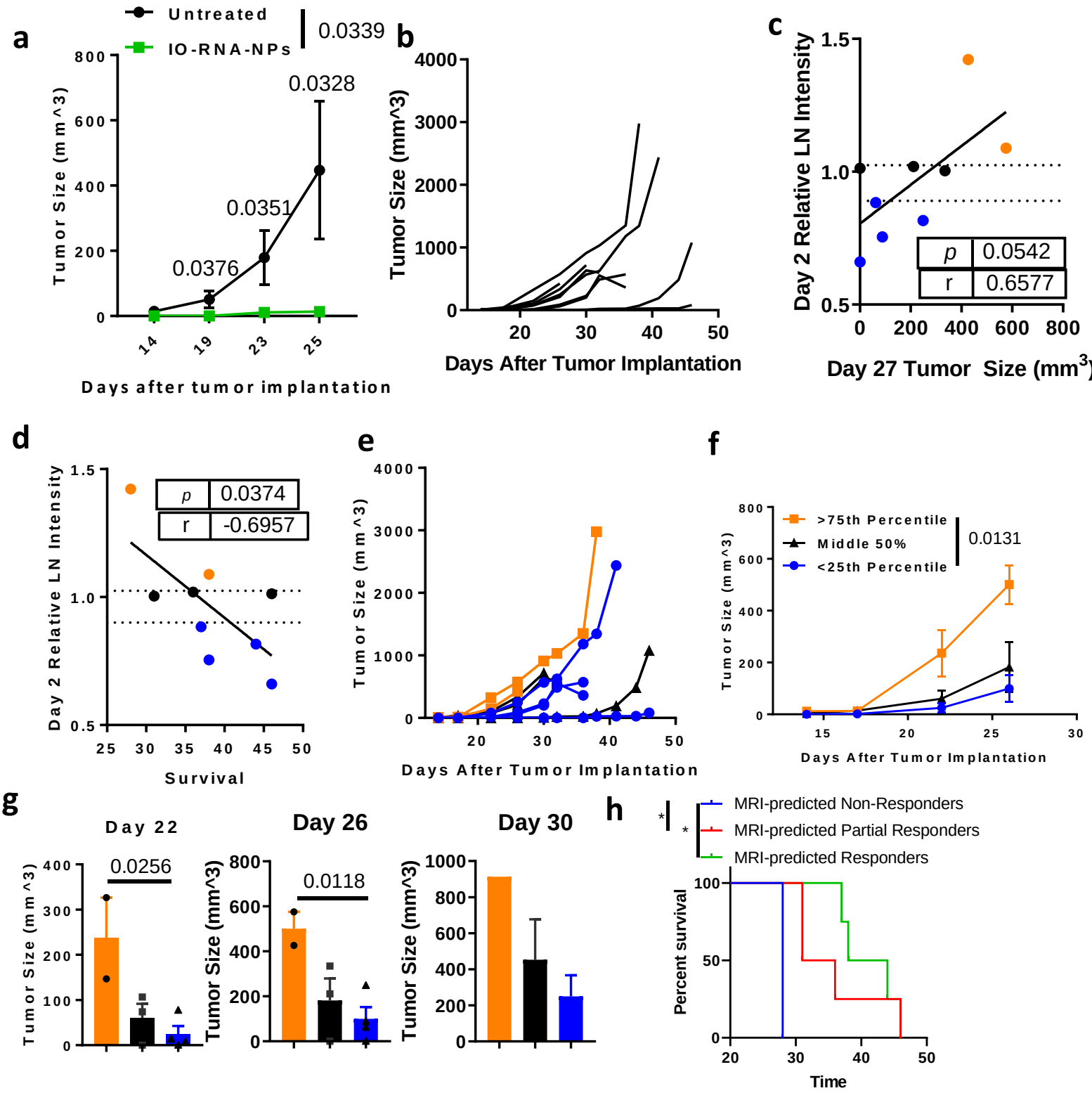

Supplementary Fig 10. MRI-detected DC migration predicts response to DC vaccines-Experiment 1. Mice with subcutaneous B16F10-OVA tumors were treated with BMDCs loaded with IO-RNA-NPs bearing ovalbumin mRNA. **a**, Tumor growth over time between treated mice (n=7) and untreated mice (*n*=5). Numbers on graph are *P* values calculated by unpaired student's t tests. **b**, Growth of individual treated tumors (n=10). **c-d,** Correlation of the relative change in MRI-detected lymph node intensity in treated compared to untreated lymph nodes (Relative LN Intensity) on Day 2 with Day 27 tumor size (**c**) and survival (**d**). Dotted lines demarcate the 25th and 75th percentiles of relative MRI intensity in lymph nodes. Datapoints from mice with substantial MRI-predicted DC migration indicated by relative VDLN intensity in the bottom 25th percentile are blue, those from mice with moderate VDLN intensity in the middle 50th percentile are black, and those from mice with high VDLN intensity in the top 75th percentile are orange. Numbers on graphs **c-d** are derived from a Pearson correlation. **e-h,** Individual tumor growth curves (**e**), summary data (**f**), tumor sizes at multiple timepoints (**g**), and survival (**h**) separated by MRI intensity on Day 2 after vaccination. Numbers on graphs are *p* values calculated from ANOVA (**f**), Mann-Whitney (**g**), or Log-Rank tests (**h**). *p<0.05.

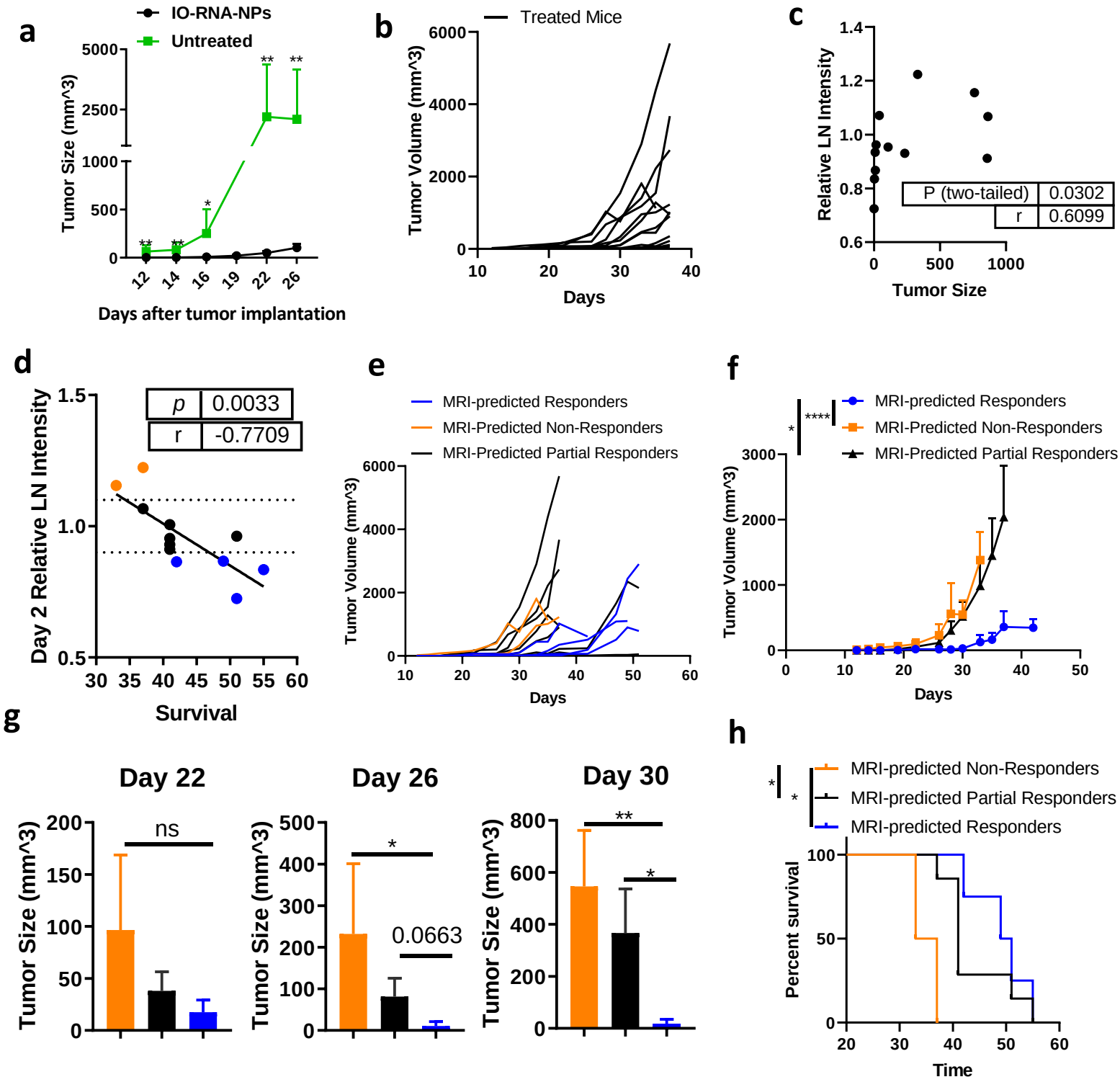

Supplementary Fig 11. MRI-detected DC migration predicts response to DC vaccines – Experiment 2. Mice with subcutaneous B16F10-OVA tumors were treated with BMDCs loaded with IO-RNA-NPs bearing ovalbumin mRNA. **a**, Tumor growth over time between treated mice (n=13) and untreated mice (*n*=2). *P* values were calculated by unpaired student's t tests. Comparison of tumor growth over time is evaluated with a two-way ANOVA. **b**, Growth of individual treated tumors separated into "responders" (n=3) and "non-responders" (n=2). **c**, Correlation of the relative change in MRI-detected lymph node intensity in treated compared to untreated lymph nodes (Relative LN Intensity) on Day 2 with Day 27 tumor size. Dotted lines demarcate the 25th and 75th percentiles of relative MRI intensity in lymph nodes. Datapoints from mice with substantial MRI-predicted DC migration indicated by relative VDLN intensity in the bottom 25th percentile are blue, those from mice with moderate VDLN intensity in the middle 50th percentile are black, and those from mice with high VDLN intensity in the top 75th percentile are orange. **d**,**e**, Correlation of Day 2 MRI-detected DC migration with tumor size (**d**) and survival (**e**). Numbers on graphs **c**-**e** represent Pearson's correlation coefficient (r) and *P* value (*p*). **f-h,** Individual tumor growth curves (**f**), summary data (**g**), and tumor sizes at multiple timepoints separated by MRI intensity on Day 2 after vaccination. Numbers on graphs are *p* values calculated from an ANOVA (**g**) and two-tailed unpaired t tests (**h**). **p<0.05, **p<0.01, ***p<0.001, ****p<0.0001.*

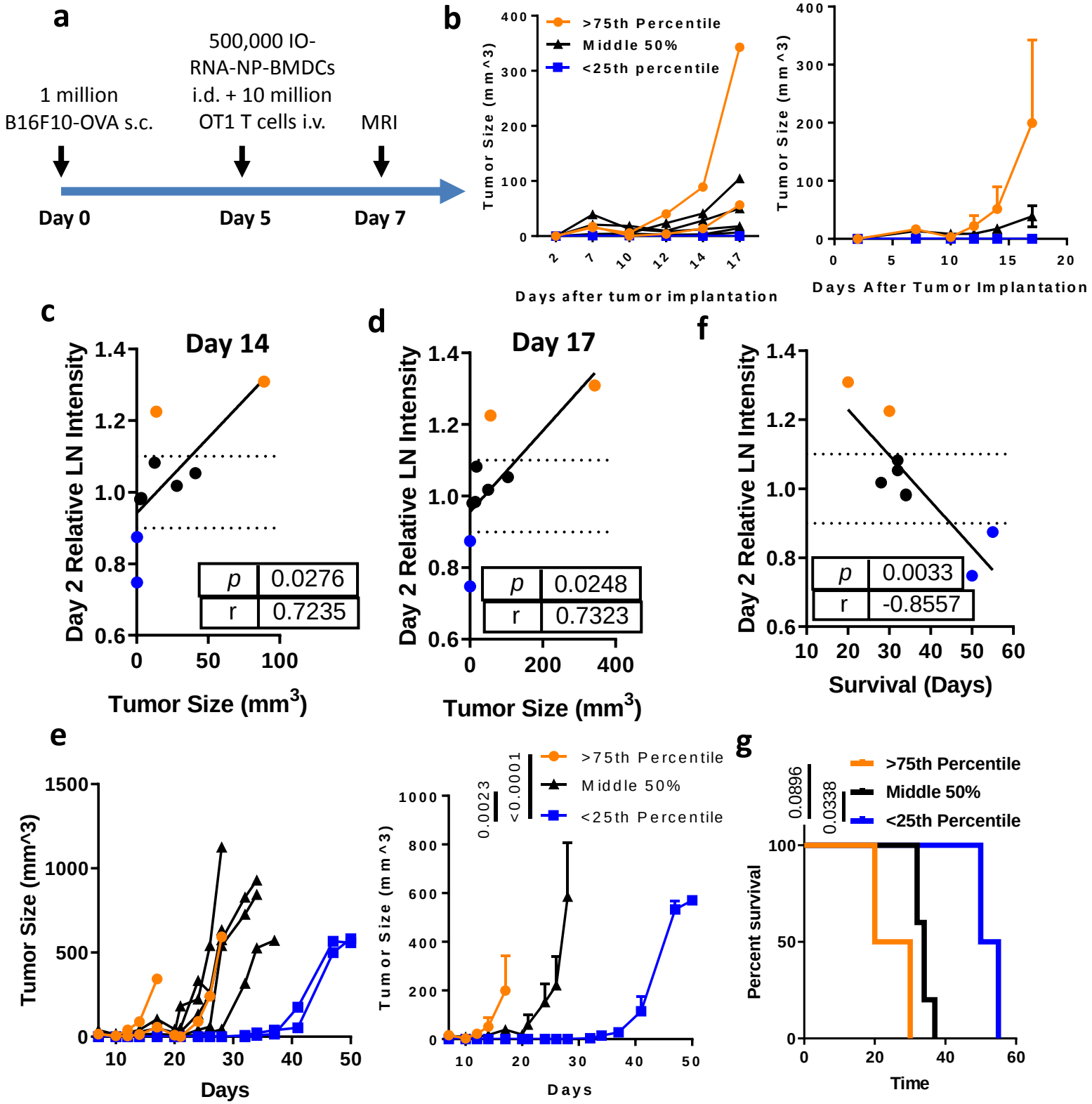

Supplementary Fig 12. MRI-detected DC migration at two days post-vaccine predicts antitumor efficacy of therapeutic DC vaccine – Experiment 1. a, Schematic of treatment schedule. Mice received subcutaneous injection of 1 million B16F10-OVA cells in the lateral flank. On Day 5 mice received intradermal (i.d.) injection of 500,000 BMDCs loaded with IO-RNA-NPs bearing OVA RNA and intravenous (i.v.) injection of 10 million OT1 T-cells. Mice were imaged with MRI after two days and followed for tumor growth and survival. **b,** Individual tumor growth curves (*left*) and summary data (*right*) for all treated mice before deaths (n=9). **c-d,** Correlation of T2*-weighted MRI intensity on Day 2 with tumor size on Day 14 (**c**) and Day 17 (**d**). Dotted lines demarcate the 25th and 75th percentiles of relative MRI intensity in lymph nodes. **e,** Individual tumor growth curves (*left*) and summary data (*right*) through deaths of all treated mice. Numbers on the graph are *p* values calculated using two-way ANOVA tests for significance. **f,** Correlation of T2*-weighted MRI intensity on Day 2 with Survival. **g,** Survival curves for all treated mice. Numbers on graph are *p* values calculated using a Log-Rank test. *P* and r values in **c, d,** and **f** are derived from a Pearson Correlation.

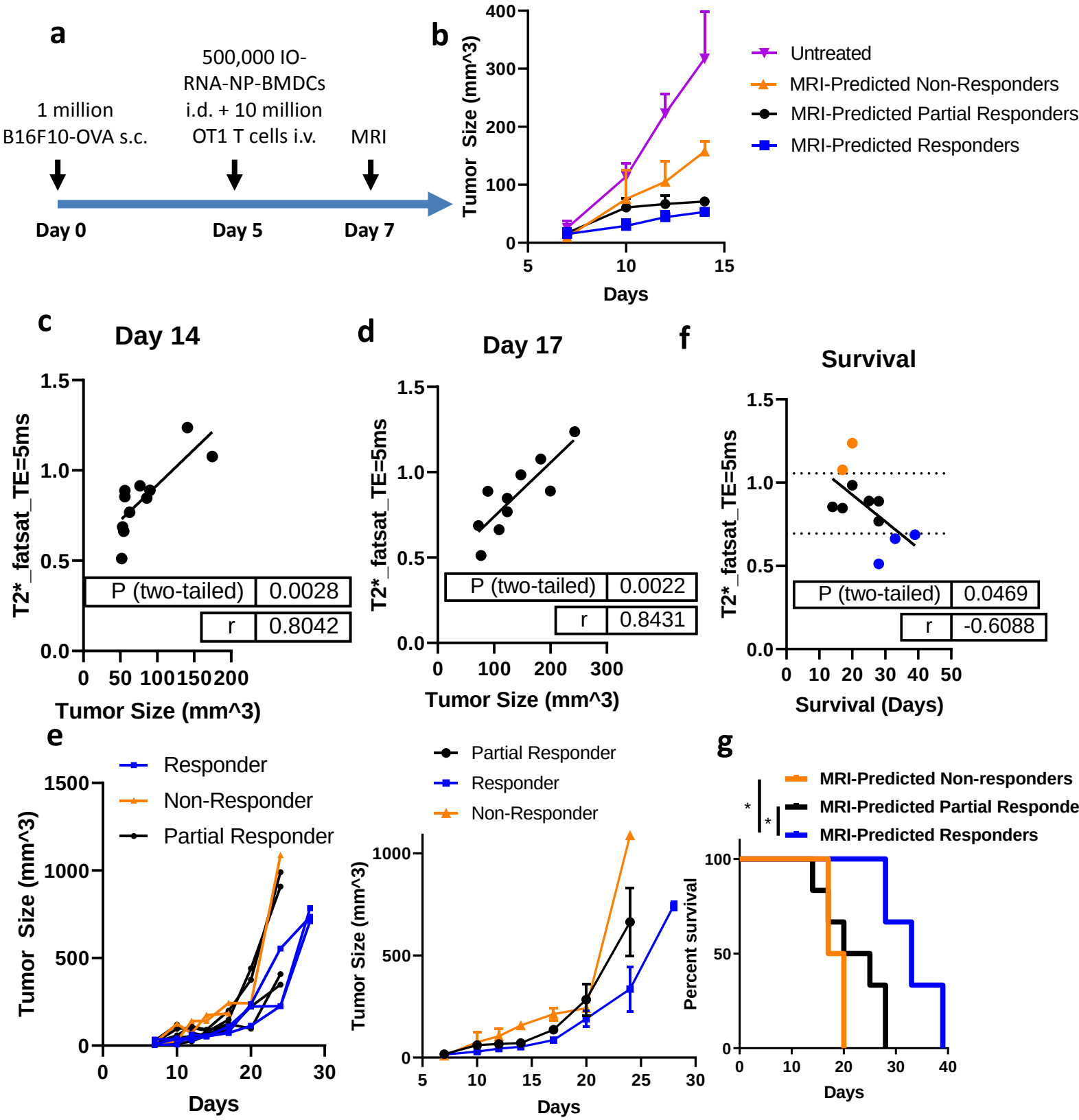

Supplementary Figure 13. MRI-detected DC migration at two days post-vaccine predicts antitumor efficacy of therapeutic DC vaccine – Experiment 2. a, Schematic of treatment schedule. Mice received subcutaneous injection of 1 million B16F10-OVA cells in the lateral flank. On Day 5 mice received intradermal (i.d.) injection of 500,000 BMDCs loaded with IO-RNA-NPs bearing OVA RNA and intravenous (i.v.) injection of 10 million OT1 T-cells. Mice were imaged with MRI after two days and followed for tumor growth and survival. **b,** Individual tumor growth curves (*left*) and summary data (*right*) for all treated mice before deaths (n=9). **c-d,** Correlation of T2*-weighted MRI intensity on Day 2 with tumor size on Day 14 (**c**) and Day 17 (**d**). Dotted lines demarcate the 25th and 75th percentiles of relative MRI intensity in lymph nodes. **e,** Individual tumor growth curves (*left*) and summary data (*right*) through deaths of all treated mice. Numbers on the graph are *p* values calculated using two-way ANOVA tests for significance. **f,** Correlation of T2*-weighted MRI intensity on Day 2 with Survival. **g,** Survival curves for all treated mice. Numbers on graph are *p* values calculated using a Log-Rank test. *P* and r values in **c, d,** and **f** are derived from a Pearson Correlation.

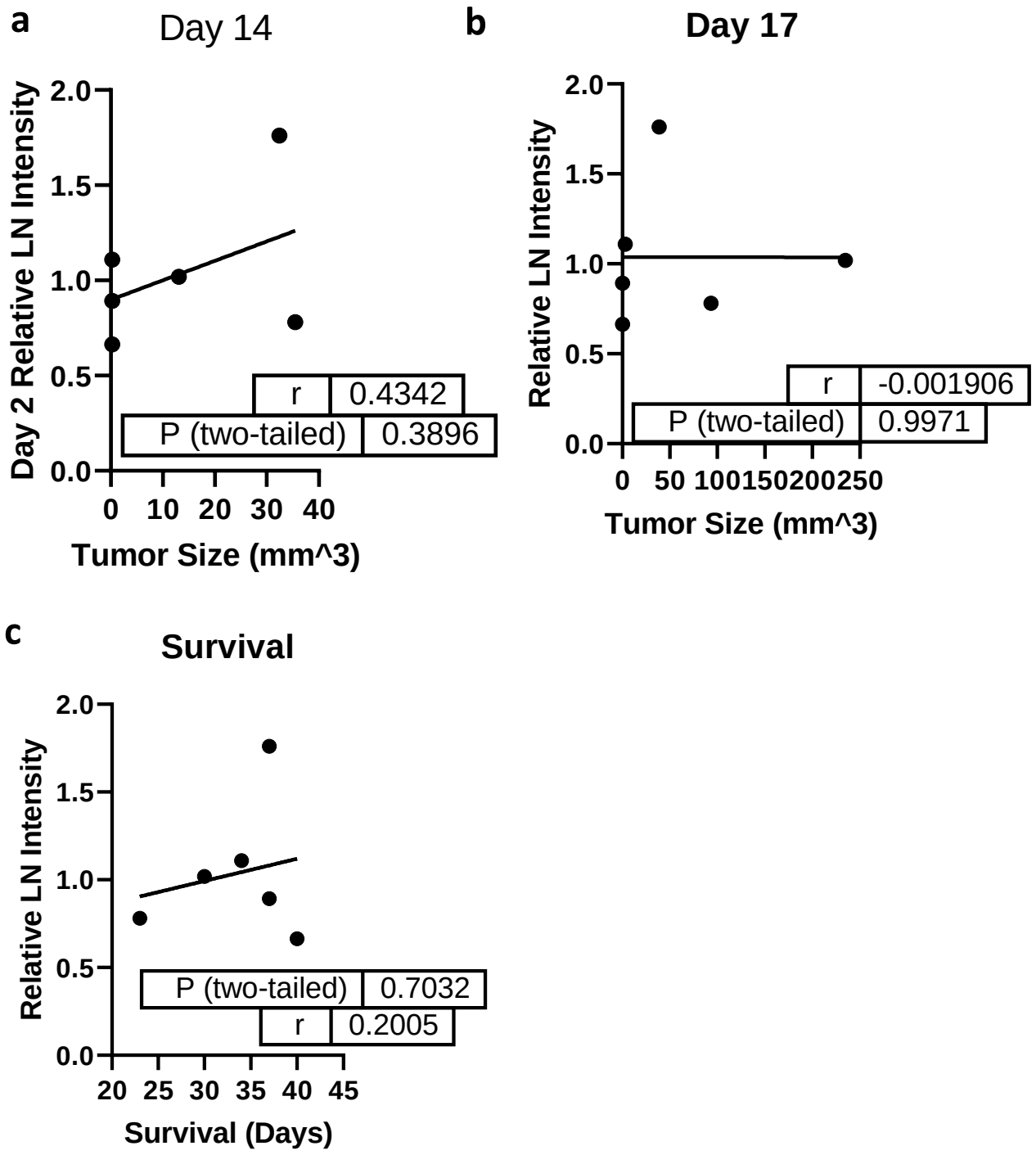

Supplementary Figure 14: LN Intensity does not predict outcome in absence of IONPs. Mice were treated with electroporated DCs 5 days after subcutaneous injection of B16F10-OVA tumors. Mice were imaged with MRI 48 hours after treatment and tumor growth was followed over time. Relative LN intensity was plotted against Day 14 tumor size (**a**), Day 17 tumor size (**b**), and survival (**c**). Numbers on graphs are correlation coefficients and p values derived from Pearson's correlation coefficient.

Formulation	GFP (%)	CD40+CD80+ CD86+ (%)	IFN-ɣ (pg/mL)	Viability (%)	Activation Score	Relative Activation Score
DOTAP	2.9	5.4	7971	57	27891	1.0
DOTAP:Chol (3:1)	5.8	21.6	18004	59	523963	18.8
DOTAP:Chol	3.8	9.8	11502	56	93794	3.4
DOTAP:DOPE	8.1	3.9	15502	55	105249	3.8
DOTAP:DMPC	0.1	4.9	120	71	17	0.0
DOTAP:DPPC	0.0	5.4	44	88	2	0.0
DOTMA	5.4	23.7	17268	53	458035	16.4
DOTMA:Chol (3:1)	5.9	15.2	10962	39	101083	3.6
DOTMA:DOPE	7.9	8.4	7805	34	45989	1.6
DOTMA:DMPC	0.0	5.1	184	54	5	0.0
DOTMA:DPPC	0.0	9.2	440	52	22	0.0
Liposomal MPL*	0.0	2.4	766	63	0	0.0
DMPC	0.0	1.6	38	67	0	0.0
Untreated	0.0	2.7	98	63	0	0.0

Supplementary Table 1: Summary data for lipid library. Liposomes were formed from the listed components at a 1:1 ratio unless otherwise noted. Summary data derived at 24 hours after incubation with BMDCs with GFP mRNA or 48 hours after incubation of OVA-transfected BMDCs with OVA-specific OT1 T cells are shown for each particle construct. Activation Score is calculated as the product of transfected cells (GFP (%)), activated cells (CD40+CD80+CD86+ (%)), viability (%), and T cell stimulating capacity (IFN-ɣ (pg/mL)). Relative Activation Scores are calculated as $(\text{Activation Score}_{\text{Sample}})/(\text{Activation Score}_{\text{DOTAP}})$.

DOTAP=1,2-dioleoyl-3-trimethylammonium-propane; Chol = Cholesterol; DOPE=1,2-dioleoyl-sn-glycero-3-phosphoethanolamine; DMPC=1,2-dimyristoyl-sn-glycero-3-phosphocholine; DPPC=1,2-dipalmitoyl-sn-glycero-3-phosphocholine; DOTMA=1,2-di-O-octadecenyl-3-trimethylammonium propane. *Liposomal MPL is a mixture of lipids and the adjuvant monophosphoryl lipid A (MLA) at a ratio of Cholesterol:DMPG:DPPC:MLA of 5.2:1.1:8.7:0.15.

Iron Oxide (ug:1mg lipid)	Particle Diameter (nm)	Zeta Potential (meV)
0	207.9 +/- 67.2	44.14 +/- 4.54
20	224.2 +/- 71.2	43.93 +/- 1.07
40	216.9 +/- 78.1	43.15 +/- 2.60
100	208.7 +/- 92.3	40.2 +/- 7.58

Supplementary Table 2: Characterization of iron oxide loaded RNA-nanoparticles. Zeta potential and diameter (measured by Nanosight) are displayed as the mean +/- the standard deviation. Results are representative summary data of three repeated experiments for each zeta potential and 4 measurements for each size. Size measurements were completed with RNA bound to liposomes. Zeta potential was measured for liposomes without RNA.

Upregulated Gene Sets	P Value
Defense Response to Virus	0.0
IFN-α Production	0.0162
Innate Immune Response	0.0035
Type I IFN Production	0.0328
TLR Signaling	0.0097
Lymphocyte migration	0.0
Positive regulation of innate immune response	0.0095

Supplementary Table 3: Gene sets upregulated after treatment with IO-RNA-NPs compared to electroporation